# Investigation of Maximum Efficiency in WPT in the MHz Band Under Varying Load and Coupling Coefficient While Satisfying ZVS


Kotaro takayama
*Faculty of Science and Technology*
*University of Science*
Noda, Japan
takayama.kotaro24@gmail.com

Luo Weisen
*Organization for Research Promotion*
*University of Science*
Noda, Japan

Tekehiro Imura
*Faculty of Science and Technology*
*University of Science*
Noda, Japan

Yoichi Hori
*Faculty of Science and Technology*
*University of Science*
Noda, Japan



*Abstract*— **The current wireless power transfer (WPT) in MHz band operation has a problem that efficiency deteriorates when the distance or load changes. To solve this problem, we will use circuit analysis to verify the maximum efficiency of WPT in MHz operation using a circuit with a class-E inverter and DC/DC converter that can handle coupling coefficient and load resistance variations, while satisfying zero-voltage switching (ZVS) and taking load and coupling coefficient into account. A system efficiency of 82.4 % was achieved in the simulation environment at a transmission frequency of 6.78 MHz with a load resistance of 10 Ω and a coupling coefficient of 0.05.**



***Keywords— Wireless power transfer (WPT), class-E inverter, megahertz (MHz), zero-voltage switching (ZVS)***


## I. INTRODUCTION

Wireless chargers are equipped with a power transmission coil on the transmitting side and a power receiving coil on the receiving side, and charge by wireless power transmission (WPT). [1]. This power transmission enables charging without cables, thus ensuring high convenience. Currently, WPTs generally transmit and receive power by setting the resonance frequency and operating frequency in the kHz band and are used in chargers and are expected to play an active role in electric vehicles [2]-[7]. However, one problem with setting the resonant frequency and operating frequency in the kHz band is the inability to downsize the equipment. To solve this problem, research is being conducted to reduce the values of devices such as capacitors and coils by setting the resonance frequency in the MHz band and performing WPT [8].

One problem with MHz-band WPTs is that, compared to kHz-band WPTs, the higher frequency requires more switching at the inverter, resulting in higher switching losses. However, this can be improved by satisfying zero-voltage switching (ZVS) and zero-derivative switching (ZDS). Another problem is that charging conditions are limited. To solve this problem, there are methods of control using an impedance matching network (IMN) or a DC/DC converter [9] [10]. The method using an IMN requires feedback control from the power receiver to the power transmitter, but the method using a DC/DC converter is more convenient because it can be completed by control on the power receiver side, eliminating the need for communication. However, while there are studies that use IMNs to find the maximum efficiency for coupling coefficient and load resistance variations, there are no studies that use DC/DC converters to find the maximum efficiency of the entire circuit [11][12].

In this paper, we use circuit analysis to demonstrate the maximum efficiency of a WPT operating in the MHz band with a class-E inverter and DC/DC converter that can handle coupling coefficient variations and load resistance variations, while satisfying ZVS and considering distance and load.

## II. CIRCUIT CONFIGURATION

### A. Circuit Configuration

Fig. 1 shows the circuit and operating waveforms.

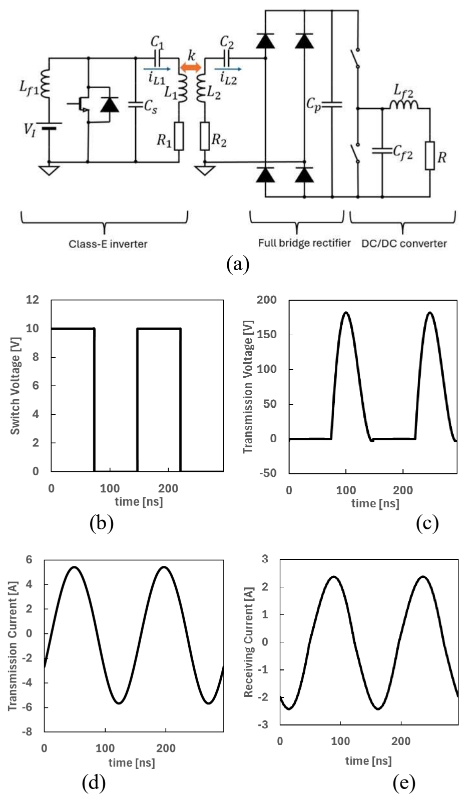


Fig. 1. (a)Design circuit and (b) Operating waveforms of the switch, (c) Voltage in the transmission section, (d) Current in the transmission section, and (e) Current in the receiving section

The circuit configuration uses a class-E inverter, a full-bridge rectifier, and a DC/DC converter. Where $V_I$ is the input voltage, $L_{f1}$ and $L_{f2}$ are both choke coils, $L_1$ and $L_2$ are the transmission coil and receiver coil, respectively, and $R_1$ and $R_2$ are the internal resistance of each coil; $C_1$ and $C_2$ are the resonant capacitors of the transformer and receiver, respectively; $C_s$ is the shunt capacitor of the class-E inverter, and $C_p$ and $C_{f2}$ are the rectifier capacitors of the full bridge rectifier and DC/DC converter, respectively. $S_1$ is a switching device operating at a duty ratio of 0.5.

### B. Prerequisite

The circuit assumes the following.

- $L_{f1}$ and $L_{f2}$ in the circuit are sufficiently large that they become choke coils and the current flowing through them is direct current.
- Consider that $C_p$ is sufficiently large that the AC component of the current flows entirely through $C_p$.
- The switch handled by the class-E inverter and DC/DC converter is ideal, with zero on resistance and infinite off resistance.
- If the currents $i_{L1}$ and $i_{L2}$ flowing in coils $L_1$ and $L_2$, respectively, are sinusoidal, consider the following

$$i_{L1} = I_{m1}\sin(\theta + \phi) \tag{1}$$

$$i_{L2} = I_{m2}\sin\left(\theta + \phi + \frac{\pi}{2}\right) \tag{2}$$

Where $I_{m1}$ and $I_{m2}$ are the amplitudes of the currents in $i_{L1}$ and $i_{L2}$, respectively, $\omega$ is the angular operating frequency, and $\phi$ is the phase shift from the gate drive voltage driving the switch of the class-E inverter.

### C. Circuit Calculations

A simplified circuit diagram of the DC/DC converter is shown in Fig. 2, with its parts represented by equivalent resistors.

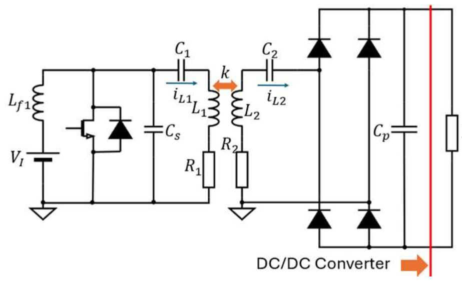


Fig. 2. Equivalent circuit with simplified DC/DC converter

The equivalent resistance $R'$ is then obtained as follows.

$$R' = \frac{R}{D_2^2} \tag{3}$$

Where $D_2$ is the duty ratio on the DC/DC converter side. A simplified equivalent circuit of the full bridge rectifier is shown in Fig. 3.

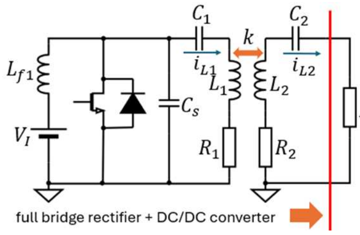


Fig. 3. Equivalent circuit with simplified full bridge rectifier

The equivalent resistance $R''$ is obtained by considering the diode loss as follows.

$$R'' = \frac{8}{\pi^2}\left(R' + \frac{\pi V_F}{I_{m2}} + \frac{\pi^2 R_F}{4}\right) \tag{4}$$

Where $V_F$ is the diode drop voltage and $R_F$ is the parasitic resistance of the diode. The final equivalent circuit is shown in Fig. 4.

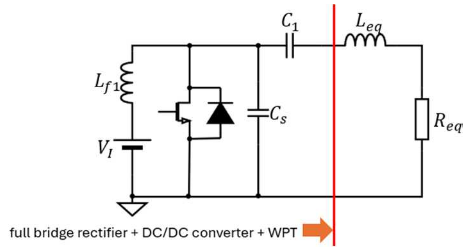


Fig. 4. The final equivalent circuit

The values of $R_{eq}$ and $L_{eq}$ that can be derived from this equivalent circuit are obtained as follows [13].

$$R_{eq} = \frac{k^2\omega^2 L_1 L_2 (R'' + R_2)}{(R'' + R_2)^2 + \left(\omega L_2 - \frac{1}{\omega C_2}\right)^2} + R_1 \tag{5}$$

$$L_{eq} = \frac{k^2 L_1\left\{(R'' + R_2)^2 - \frac{L_2}{C_2} + \left(\frac{1}{\omega C_2}\right)^2\right\}}{(R'' + R_2)^2 + \left(\omega L_2 - \frac{1}{\omega C_2}\right)^2} + L_1(1 - k^2) \tag{6}$$

Where $k$ is coupling coefficient. To make this equivalent circuit a circuit that achieves the ZVS condition

$$v_s(2\pi) = 0 \tag{7}$$

must be satisfied. Where $v_s$ is the switching voltage. The values of the components required from the previous study are as follows [14]. Also, from previous study [14], $v_s$ is is also obtained as follows.

$$v_s = \int_0^{2\pi} i_{Cs}\, d(\omega t) = \begin{cases} 0 \ (0 < \omega t \le 2\pi D_1) \\ \dfrac{I_I(\omega t - 2\pi D_1) + I_{m_1}[\cos(\omega t + \phi) - \cos(2\pi D_1 + \phi)]}{\omega C_1} \\ (2\pi D_1 < \omega t \le 2\pi) \end{cases} \tag{8}$$

where $I_I$ is the current flowing in choke coil $L_{f1}$. Also, $i_{C1}$ is the current flowing in $C_s$ and is obtained as follows.

$$i_{C_s} = \begin{cases} 0 \ (0 < \omega \leq 2\pi D_1) \\ I_I - I_{m_1}\sin(\omega t + \phi) \ (2\pi D_1 < \omega t \leq 2\pi) \end{cases} \quad (9)$$

From equation (8), $I_{m_1}$ is obtained as follows.

$$I_{m_1} = I_I \frac{2\pi(1 - D_1)}{\cos(2\pi D_1 + \phi) - \cos\phi} \quad (10)$$

The input voltage $V_I$ also has the following relationship.

$$V_I = \frac{1}{2\pi}\int_0^{2\pi} v_s \, d(\omega t) = \frac{(1 - D_1)D'}{\omega C_1 \tan(\pi D_1 + \phi)\sin\pi D_1} I_I \quad (11)$$

$D'$ is the following value.

$$D' = [(1 - D_1)\pi\cos\pi D_1 + \sin\pi D_1] \quad (12)$$

The amplitude of the voltage $V_{R_{eq}}$ of the equivalent resistance $R_{eq}$ is obtained from equation (8) as follows.

$$V_{R_{eq}} = \frac{1}{\pi}\int_0^{2\pi} v_s \sin(\omega t + \phi)\, d(\omega t) = -\frac{2\sin\pi D_1 \sin(\pi D_1 + \phi)}{\pi(1 - D_1)} V_I \quad (13)$$

Where $L_b$ is the reactance component left over when $L_{eq}$ and $C_1$ cancel each other out due to resonance. This give $C_1$, $C_S$, and output power $P_{out}$ as follows.

$$C_S = \frac{2\sin\pi D_1 \cos(\pi D_1 + \phi)\sin(\pi D_1 + \phi)\, D'}{\pi^2(1 - D_1)\omega R_{eq}} \quad (14)$$

$$C_1 = \frac{1}{\omega^2(L_{eq} - L_b)} \quad (15)$$

$$P_{out} = \frac{4R'k^2L_1L_2\omega^2}{\pi^2(R'' + R_2)^2} I_{m1}^2 \quad (16)$$

The efficiency $\eta$ is also obtained as follows

$$P_{R_1} = \frac{R_1}{2} I_{m1}^2 \quad (17)$$

$$P_{R_2} = \frac{R_2 k^2 L_1 L_2 \omega^2}{2(R'' + R_2)^2} I_{m1}^2 \quad (18)$$

$$P_D = \frac{4V_F}{\pi}\left(\frac{k\sqrt{L_1L_2}\omega}{R'' + R_2} I_{m1}\right) + \frac{R_F k^2 L_1 L_2 \omega^2}{2(R'' + R_2)^2} I_{m1}^2 \quad (19)$$

$$\eta = \frac{P_{out}}{P_{out} + P_{R_1} + P_{R_2} + P_D} \quad (20)$$

Where $P_{R1}$, $P_{R_2}$, and $P_D$ are the losses at $R_1$, $R_2$, and $R_D$, respectively. From these values, the optimal parameters can be obtained.

## III. Maximum Efficiency

In this section, we confirm by simulation whether the maximum efficiency can be achieved by considering the load and coupling coefficient while satisfying ZVS in WPT in MHz band operation in a circuit using a class-E inverter and DC/DC converter that can handle load and coupling coefficient variations. Table 1 shows the components of the circuit.

TABLE I Parameter value.

| Components | Theoretical value | Simulation |
|---|---|---|
| $f$ | 6.78 MHz | 6.78 MHz |
| $V_I$ | 50 V | 50 V |
| $D_1$ | 0.5 | 0.5 |
| $V_F$ | 0.7 V | 0.7 V |
| $R_F$ | 0.5 Ω | 0.5 Ω |
| $R_1$ | 0.5 Ω | 0.5 Ω |
| $R_2$ | 0.5 Ω | 0.5 Ω |
| $L_1$ | 5 μH | 5 μH |
| $L_2$ | 5 μH | 5 μH |
| $C_2$ | 110 pF | 110 pF |
| $L_{f1}$ | - | 500 μF |
| $L_{f2}$ | - | 500 μF |
| $C_{f2}$ | - | 4.7 μF |
| $C_p$ | - | 4.7 μF |

### A. Maximum Efficiency under ZDS Conditions

To achieve ZDS by previous studies

$$\left.\frac{dv_s}{d(\omega t)}\right|_{\omega t = 2\pi} = 0 \quad (21)$$

must be satisfied [14]. This allows $\phi$ to be

$$\tan\phi = \frac{\cos 2\pi D_1 - 1}{2\pi(1 - D_1) + \sin 2\pi D_1} \quad (22)$$

must satisfy. From this equation, $C_1$ and $C_S$ can be obtained by setting $R_{eq}$. Fig. 5 shows the analytical waveforms of the output power and efficiency for coupling coefficients $k = 0.01$, 0.05 and 0.1 based on the theoretical equation and the simulation results. However, the load resistance is 10 Ω, which limits the $R_{eq}$ that can be taken in the simulation. Since $R_{eq}$ includes the internal resistance of the power transmission unit, the minimum value is $R_{eq} = 0.5$. In addition, $C_S$ and $C_1$ are modified every time to their optimal values using equations (14) and (15).

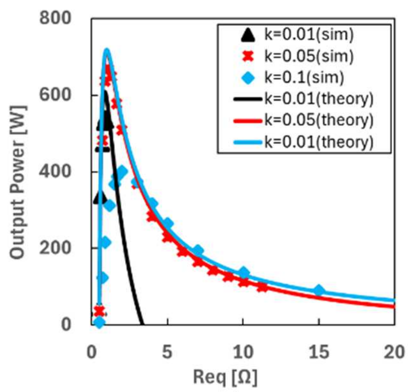

(a)

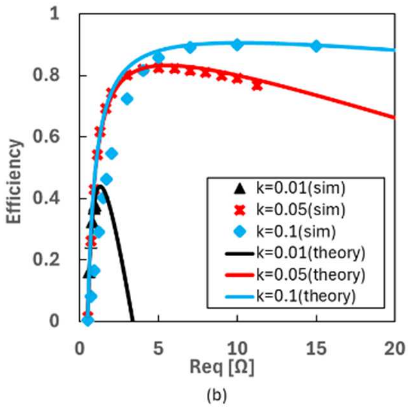


Fig. 5. Design curve of (a) Output power, and (b) Efficiency, as functions of $R_{eq}$ with fixed coupling coefficients.

From Fig. 5, the maximum efficiency points of the analytical waveforms of the theoretical and simulation results coincide. However, when $R_{eq}$ is small, the results from the theoretical equation and the simulation do not match. The reason for this is thought to be that when $R_{eq}$ is small, the load resistance of the power receiver, which is inversely proportional to $R_{eq}$ in equation (5), becomes too large, resulting in a small Q value, and the sinusoidal condition is not satisfied.

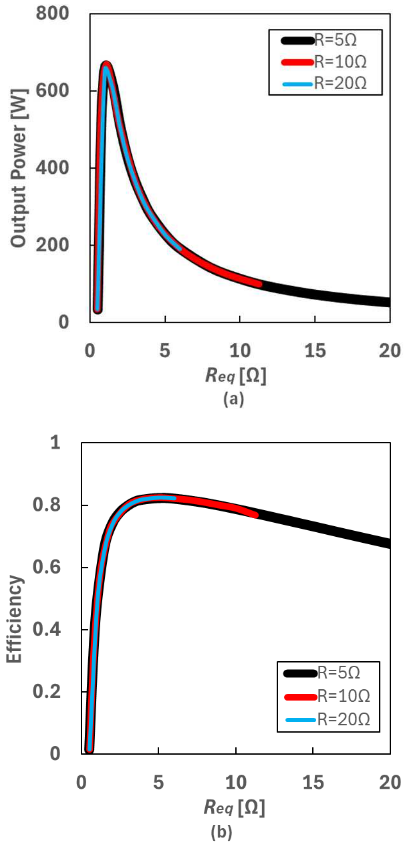


Fig. 6. Design curve of (a) Output power, and (b) Efficiency, as functions of $R_{eq}$ with fixed load resistances.

Fig. 6 shows the efficiency and output power when k=0.05 and the load fluctuates. As shown in this figure, although the range of $R_{eq}$ changes when the load resistance fluctuates, $R_{eq}$ can be set to any value by changing the duty ratio of the DC/DC converter, and when $R_{eq}$ is equal, the efficiency and output power hardly change even if the load resistance is different. Therefore, the use of a DC/DC converter allows the system to cope with load fluctuations.

*B. Maximum Efficiency without ZDS Condition*

In the calculations, power efficiency and other factors were considered by fixing $\phi$ to be ZDS, but in considering maximum efficiency, it is necessary to consider power efficiency when ZDS is not considered. For this purpose, $\phi$ in equation (22) are rederived as following equations. This makes $C_s$ a degree of freedom.

$$\phi = \frac{1}{2}\arcsin\left(\frac{\pi^2(1-D_1)\omega C_s R_{eq}}{D'}\right) + \pi(1-D_1) \qquad (23)$$

$$\phi = -\frac{1}{2}\arcsin\left(\frac{\pi^2(1-D_1)\omega C_s R_{eq}}{D'}\right) + \pi\left(\frac{3}{2}-D_1\right) \qquad (24)$$

This makes $C_s$ a degree of freedom.

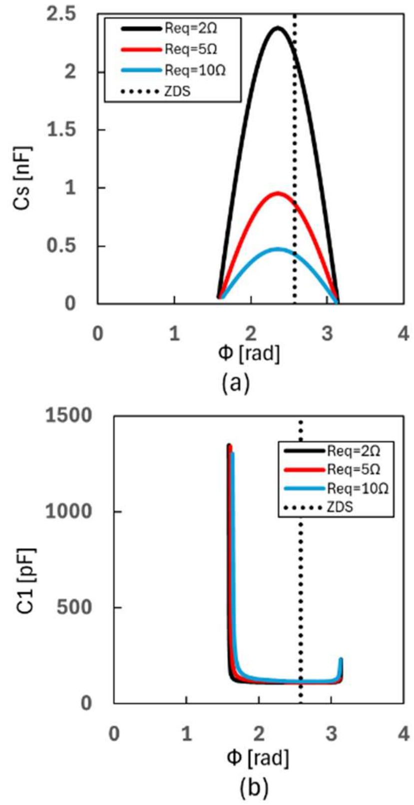


Fig. 7. Design curve of (a) $C_s$, and (b) $C_1$, as functions of Φ with fixed $R_{eq}$.

Fig. 7 shows the change in $C_s$ and $C_1$ when the same circuit configuration as in section A is used. This makes it possible to vary the value of $\phi$ by changing $C_s$ and $C_1$.

From Fig. 5, when the coupling coefficient is 0.1, the efficiency is maximum when $R_{eq}$ is 10 Ω. When the value of $\phi$ is changed as shown in Fig. 7 at that component value, the analytical waveforms of the results from the theoretical equation and the simulation are shown in Fig. 8.

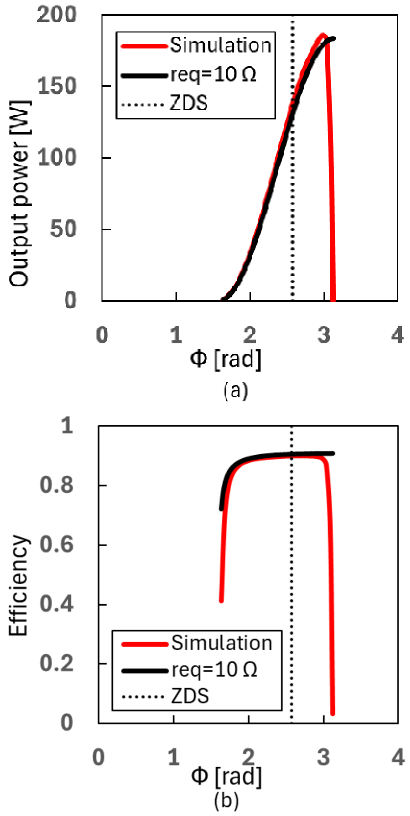


Fig. 8. Design curve of (a) Output power, and (b) Efficiency, as functions of Φ.

From Fig. 8, both output power and efficiency improve as the value of $\phi$ is increased. However, in the range beyond ZDS, the best performance is achieved when ZDS is satisfied because of the reverse voltage on the diode of the class-E inverter during ZVS. It can also be seen that the theoretical equation and the simulation do not match when approaching the limit of the range of $\phi$. This is because the value of $L_b$ becomes smaller as $C_1$ becomes smaller, as can be seen from equation (15), and the $Q$ value on the transmission side becomes smaller, so the sine wave condition is not satisfied.

## IV. Conclusion

In this paper, a circuit analysis is performed for the maximum efficiency in a WPT in MHz band operation with a class-E inverter and a DC/DC converter that can handle load and coupling coefficient variations while satisfying ZVS and considering coupling coefficient and load resistance. The analysis showed that the maximum efficiency can be obtained by changing the $R_{eq}$ and duty ratio, even when the coupling coefficient and load resistance are varied, based on the theoretical equations and simulation results. In the simulation environment, a system efficiency of 82.4% was achieved at a transmission frequency of 6.78 MHz, a load resistance of 10 Ω, and a coupling factor of 0.05.

Also, if ZDS is removed from the condition, there is one more degree of freedom, but the efficiency is best when ZDS is used, so it is better to use a circuit that satisfies the ZDS condition even when designing for maximum efficiency.

This technology can be applied in a variety of locations. For example, in EV charging, it has the potential to accurately charge vehicles at maximum efficiency even when there is a difference in vehicle height or when the ground slope is not level. Future research should include experiments with actual equipment to determine the potential for use in various locations, such as EV charging.


[1] X. Lu, P. Wang, D. Niyato, D. I. Kim, and Z. Han, "Wireless Charging Technologies: Fundamentals, Standards, and Network Applications," *IEEE Commun. Surveys Tuts*, vol. 18, no. 2, pp. 1413-1452, Secondquarter 2016.

[2] T. Imura and Y. Hori, "Maximizing Air Gap and Efficiency of Magnetic Resonant Coupling for Wireless Power Transfer Using Equivalent Circuit and Neumann Formula," *IEEE Trans. Ind. Electron.*, vol. 58, no. 10, pp. 4746-4752, Oct. 2011.

[3] R. Zhang and C. K. Ho, "MIMO Broadcasting for Simultaneous Wireless Information and Power Transfer," *IEEE Trans. Wireless Commun.*, vol. 12, no. 5, pp. 1989-2001, May 2013.

[4] S. Moon, B. -C. Kim, S. -Y. Cho, C. -H. Ahn, and G. -W. Moon, "Analysis and Design of a Wireless Power Transfer System With an Intermediate Coil for High Efficiency," *IEEE Trans. Ind. Electron.*, vol. 61, no. 11, pp. 5861-5870, Nov. 2014.

[5] Y. Jang and M. M. Jovanovic, "A contactless electrical energy transmission system for portable-telephone battery chargers," *IEEE Trans. Ind. Electron.*, vol. 50, no. 3, pp. 520-527, June 2003.

[6] C. Wang, O. H. Stielau, and G. A. Covic, "Design considerations for a contactless electric vehicle battery charger," *IEEE Trans. Ind. Electron.*, vol. 52, no. 5, pp. 1308-1314, Oct. 2005.

[7] J. Sallan, J. L. Villa, A. Llombart, and J. F. Sanz, "Optimal Design of ICPT Systems Applied to Electric Vehicle Battery Charge," *IEEE Trans. Ind. Electron.*, vol. 56, no. 6, pp. 2140-2149, June 2009.

[8] Y. Wang, Z. Sun, Y. Guan, and D. Xu, "Overview of Megahertz Wireless Power Transfer," *Proc. IEEE*, vol. 111, no. 5, pp. 528-554, May 2023.

[9] Y. Shao, H. Zhang, M. Liu, and C. Ma, "Explicit Design of Impedance Matching Networks for Robust MHz WPT Systems With Different Features," *IEEE Trans. Power Electron.*, vol. 37, no. 9, pp. 11382-11393, Sept. 2022.

[10] Y. Komiyama, A. Komanaka, H. Ota, Y. Ito, T. Mishima, T. Uematsu, A. Konishi, W. Zhu, K. Nguyen, and H. Sekiya, "Analysis and Design of High-Frequency WPT System Using Load-Independent Inverter With Robustness Against Load Variations and Coil Misalignment," *IEEE Access*, vol. 12, pp. 23043-23056, 2024.

[11] Y. Shao, N. Kang, H. Zhang, R. Ma, M. Liu, and C. Ma, "A Lightweight and Robust Drone MHz WPT System via Novel Coil Design and Impedance Matching," *IEEE Trans. Ind. Appl.*, vol. 59, no. 3, pp. 3851-3864, May-June 2023.

[12] Y. Liu and H. Feng, "Maximum Efficiency Tracking Control Method for WPT System Based on Dynamic Coupling Coefficient Identification and Impedance Matching Network," *IEEE J. Emerg. Sel. Top. Power Electron.*, vol. 8, no. 4, pp. 3633-3643, Dec. 2020.

[13] T. Nagashima, X. Wei, E. Bou, E. Alarcón, M. K. Kazimierczuk, and H. Sekiya, "Steady-State Analysis of Isolated Class-E2 Converter Outside Nominal Operation," *IEEE Trans. Ind. Electron.*, vol. 64, no. 4, pp. 3227-3238, Apr. 2017.

[14] M. K. Kazimierczuk and D. Czarkowski, "*Resonant Power Converters*," Wiley, Second Edition 2011.